Controlling the Assembly of UreidoPyrimidinone Supramolecular Monomers by Tuning the Hydrophilic Hydrophobic Balance

Journal of Polymer Science

WILEY

JOURNAL OF POLYMER SCIENCE

RESEARCH ARTICLE OPEN ACCESS

Controlling the Assembly of Ureido-Pyrimidinone Supramolecular Monomers by Tuning the Hydrophilic-Hydrophobic Balance

Riccardo Bellan[1,2] | Annalisa Cardellini[3] | Claudio Perego[3,4] | Lars J. M. M. Paffen[1,5] | Laura Rijns[1,2] | Giovanni M. Pavan[4] | Patricia Y. W. Dankers[1,2,5]

[1]Institute for Complex Molecular Systems, Eindhoven University of Technology, Eindhoven, the Netherlands | [2]Department of Biomedical Engineering, Eindhoven University of Technology, Eindhoven, the Netherlands | [3]Department of Innovative Technologies, University of Applied Sciences and Arts of Southern Switzerland, Lugano, Switzerland | [4]Department of Applied Science and Technology, Politecnico di Torino, Torino, Italy | [5]Department of Chemical Engineering and Chemistry, Eindhoven University of Technology, Eindhoven, the Netherlands

Correspondence: Patricia Y. W. Dankers (p.y.w.dankers@tue.nl)

Received: 6 September 2025 | **Revised:** 26 October 2025 | **Accepted:** 27 October 2025

Funding: This work was supported by the Ministerie van Onderwijs, Cultuur en Wetenschap (024.005.020), the Nederlandse Organisatie voor Wetenschappelijk Onderzoek (VI.C.222.088), and the HORIZON EUROPE Framework Programme (101079482).

Keywords: cryoTEM | molecular dynamics simulations | self-assembly | supramolecular polymers | ureido-pyrimidinone

ABSTRACT

Understanding the self-assembly of supramolecular monomers in water is essential to develop responsive and bioactive biomaterials. In this work, a series of water-compatible ureido-pyrimidinone (UPy) derivatives differing in the length of the oligo(ethylene glycol) chain and of the alkyl-urea spacer are prepared. The self-assembly behavior of each monomer is elucidated in water by means of experimental techniques and computational molecular modeling, unveiling the importance of the monomer hydrophilic-hydrophobic balance in the self-assembly properties and morphology of the resulting supramolecular polymers. Even though the increasing size of the alkyl-urea spacer is shown to foster both the UPy dimerization and the π–π stacking of the dimers, molecular dynamics simulations highlight a competitive intramolecular interaction between the UPy core and the lateral urea moiety, leading to the formation of sheet-like structures rather than one-dimensional supramolecular polymers in water. The findings of this work highlight the importance of monomer design on the self-assembly properties of UPy systems, paving the way towards the development of novel supramolecular biomaterials with tuneable properties.

1 | Introduction

Supramolecular polymers are emerging as promising candidates to interact with or guide cellular behavior owing to their high modularity, which allows for extensive and orthogonal control over many of their properties [1]. To better understand and efficiently fabricate these systems, it is important to study their self-assembly in water, where a delicate balance between the polar and apolar molecular fragments is needed to optimize both their aggregation and water solubility [2]. Systematic investigations on the effect of chemical modifications of supramolecular building blocks on their self-assembly are therefore essential to establish solid structure–assembly relationships. The consequent control over the assembly process through proper monomer design enables, in turn, tuning the morphology and molecular dynamics of the supramolecular polymers in water, features that have been shown to play a crucial role for bioactivity at the cell-material interface [3–6]. Specifically, the dynamics of supramolecular constructs have been shown to regulate the receptor–ligand interactions by allowing optimal distribution of

the ligand along the supramolecular scaffold [4, 6]. Conversely, their morphology has been demonstrated to control not only the ligand–target interactions but also cellular death [7, 8].

In linear supramolecular monomers, the effects of modifying the hydrophilic-hydrophobic balance on the self-assembly properties and morphology of the resulting supramolecular structures have been deeply investigated. Among these, peptide amphiphiles (PAs) represent an established class of supramolecular building blocks that self-assemble into high-aspect ratio nanofibers in solution, with their morphology and dynamics dictated by the peptide sequence [4, 6]. In this context, Cui *et al.* [9] demonstrated that alternating a hydrophobic valine (Val) and a hydrophilic glutamic acid (Glu) within the peptide sequence of PAs promotes the formation of large belt-like structures without curvatures in water. Conversely, PAs containing Val residues exhibit a high propensity to form rigid β-sheets, whereas the incorporation of more hydrophilic amino acids, such as alanine (Ala) and glycine (Gly), within the peptide sequence leads to more dynamic and disordered structures [10–14]. In comparison, Liu *et al.* [15] reported on the morphological transition of bis-urea bolaamphiphiles from spherical micelles to rod-like fibers by tuning the length of both the hydrophobic and hydrophilic moieties within the supramolecular monomers. Another notable class of supramolecular monomers is 1,3,5-benzene-tricarboxamide (BTA) molecules, which form one-dimensional (1D) supramolecular polymers in water through a combination of π–π stacking, hydrophobic interactions and hydrogen bonding between the amides [16, 17]. Leenders *et al.* [2] established a structure-assembly relationship for BTA molecules in water by systematically varying the length of the alky spacer flanked by the tetra(ethylene glycol) chains and the aromatic core. Their findings revealed the necessity of at least 11 methylene units in the alky spacers to promote intermolecular hydrogen bonding between the amides and the consequent formation of one-dimensional (1D) supramolecular polymers in water. Moreover, Hendrikse et al. [18] investigated the effect of the tetra(ethylene glycol) substitution with mono- and disaccharides on the self-assembly of BTAs in water, showing 1D fibers formation with monosaccharides and spherical micelles when disaccharides were introduced. All these studies emphasize the critical role of the monomer design in determining the self-assembly properties and the morphology of the resulting supramolecular polymers in water.

Our laboratory has ample experience in ureido-pyrimidinone (UPy) molecules to fabricate supramolecular biomaterials for drug delivery [19–21] and regenerative medicine [22, 23]. UPy molecules have been shown to dimerize through a self-complementary donor-donor-acceptor-acceptor (DDAA) hydrogen bonding array in various organic solvents [24]. The resulting dimers can assemble further the dimeric state by forming a flat surface that promotes π–π stacking and enables the formation of 1D supramolecular polymers, stabilized by additional lateral hydrogen bonding provided by an alkyl urea moiety [25]. To extend their application in the biomedical field, water-compatible UPy molecules have been developed by coupling the UPy motif to hydrophilic poly(ethylene glycol) (PEG) chains. However, an additional alkyl spacer flanked by the lateral urea and the hydrophilic periphery is required to protect the hydrogen bonding units from water penetration [26, 27]. The resulting supramolecular UPy monomers (UPy-C_6-U-C_{12}-Ut-PEG) have been shown to self-assemble into high-aspect ratio elongated structures in aqueous media, with morphology and molecular dynamics depending on the length of the PEG chain and the alkyl-urea spacer tethered to it [27, 28]. Indeed, Hendrikse *et al.* [27] reported the formation of robust and stable μm-long fibers for a UPy molecule equipped with a monodisperse undeca(ethylene glycol) at the periphery, whereas nm-long dynamic fibers have been observed for a telechelic bifunctional UPy molecule featuring a polydisperse PEG with a molecular weight of ~20 kDa, as a result of both an entropic and steric effect. Conversely, Bellan *et al.* [28], demonstrated that increasing the length of the alkyl-urea spacer, and thus the overall hydrophobicity of the monomers, promotes more efficient self-assembly in water, fiber bundling, and enhances cell adhesion and spreading in both 2D and 3D culture.

Despite the above-mentioned studies and the extensive use of UPy as biomaterials, opportunities remain to systematically elucidate the role of each individual molecular component in governing their self-assembly in aqueous environments. In this regard, de Greef *et al.* [29, 30] investigated the effect of oligo(ethylene glycol) chains of varying lengths on the dimerization constant (K_{dim}) of UPy molecules in chloroform. They found that substituting UPy molecules with OEG chains connected via a C_2 spacer results in a 1000-fold drop in K_{dim} compared to aliphatic-substituted UPy, as a consequence of competitive hydrogen-bond-induced backfolding of the OEG chain to the urea group within the UPy ring [24]. Moreover, while the K_{dim} decreases with the increase in ethylene glycol units, extending the length of the alkyl spacer between the UPy unit and the OEG chain leads to a rise in K_{dim}.

Inspired by the work of de Greef *et al.* [29, 30], this study presents a comprehensive investigation into the influence of varying both the OEG chain length and the alkyl spacer connecting it to the UPy unit on the supramolecular polymerization of the resulting monomers in water. To this end, three classes of UPy derivatives connected to monodisperse OEG chains of varying length directly or via an alkyl-urea spacer are synthesized and fully characterized. The self-assembly behavior of the resulting supramolecular monomers in water is explored in great detail both experimentally and through molecular dynamics (MD) simulations, to gain more details into the contribution of each molecular fragment in the assembly process. The findings of this work demonstrate that the increasing size of the alkyl spacer enhances the self-assembly of the various monomers in water, while the increasing number of ethylene glycol units at the periphery improves their water solubility and the mobility of the assemblies in solution.

2 | Results and Discussion

2.1 | Design and Synthesis

The monomers design takes inspiration from the work of de Greef *et al.* [29, 30] To investigate the impact of the hydrophilic-hydrophobic balance, or so-called hydrophilic–lipophilic balance (HLB), on the self-assembly behavior of UPy molecules, three distinct classes of monomers have been synthesized (Scheme 1).

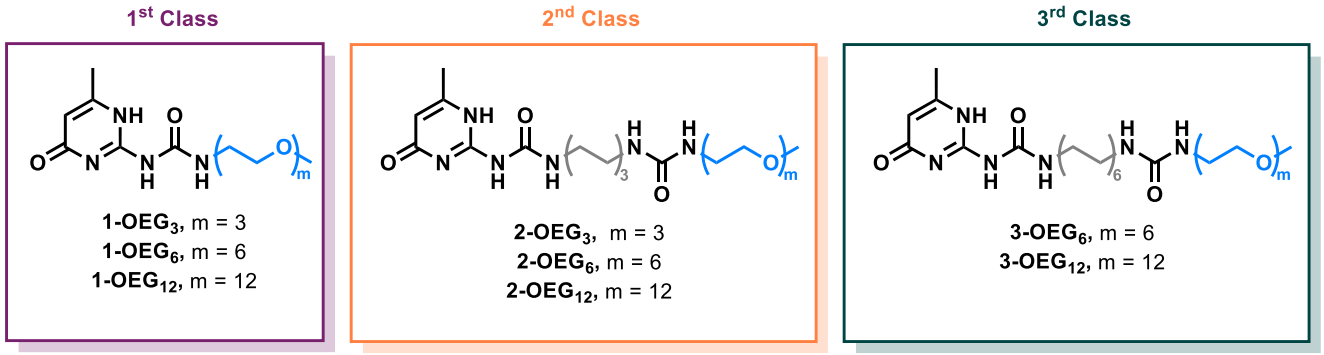

SCHEME 1 | Chemical structure of the monomers used in this study. Varying chemical moieties are labeled with different colors (alkyl-urea spacers in gray and OEG chains in blue).

TABLE 1 | HLB values of each monomer calculated through Griffin's method [31].

Monomer	1-OEG$_3$	1-OEG$_6$	1-OEG$_{12}$	2-OEG$_3$	2-OEG$_6$	2-OEG$_{12}$	3-OEG$_6$	3-OEG$_{12}$
HLB	10.3	13.2	15.7	7.1	10	13.1	8.7	11.9

These molecules feature monodisperse OEG chains of varying length (blue part), attached to the UPy motif either directly or through an alkyl-urea spacer (gray part) comprising 6 or 12 methylene units, resulting in different hydrophilic–lipophilic balance (HLB) values (Table 1). The first class (**1-OEG$_m$**) includes three UPy derivatives functionalized with monomethyl tri(ethylene glycol) (**1-OEG$_3$**), monomethyl hexa(ethylene glycol) (**1-OEG$_6$**), or monomethyl dodeca(ethylene glycol) (**1-OEG$_{12}$**). Similarly, the second class (**2-OEG$_m$**) consists of three monomers featuring tri(ethylene glycol) (**2-OEG$_3$**), monomethyl hexa(ethylene glycol) (**2-OEG$_6$**), or monomethyl dodeca(ethylene glycol) (**2-OEG$_{12}$**), but connected to the UPy moiety via an alkyl-urea spacer of 6 methylene units (C_6). Lastly, the third class (**3-OEG$_m$**) comprises two derivatives where the UPy unit is linked either to monomethyl hexa(ethylene glycol) (**3-OEG$_6$**) or monomethyl dodeca(ethylene glycol) (**3-OEG$_{12}$**) via a 12-methylene (C_{12}) alkyl-urea spacer. Notably, in all three classes, the HLB values increase with the number of ethylene glycol units within the OEG chain.

The synthesis of the three classes of UPys is facile and efficient (Scheme S1), consisting of two synthetic steps adapted from the literature [26, 32] and easy purification methods, allowing the isolation of the final products through normal phase flash column chromatography in good yields (65%–98%). The synthesis of **1-OEG$_m$** is achieved by activating the amino group of the 6-methyl-isocytosine (**6**) with 1,1′-carbonyldiimidazole, providing the active ester (**4**) which is reacted with the respective monomethyl ethylene oxide amine (**mOEG$_m$-NH$_2$**) to provide the final compounds in nearly quantitative yields (92%–98%). Conversely, the synthesis of **2-OEG$_m$** and **3-OEG$_m$** is pursued by reacting the amino group of **6** with the respective diisocyanate alkyl chain (hexamethylene diisocyanate for **2-OEG$_m$** and 1,12-diisocyanatedodecane for **3-OEG$_m$**) followed by the coupling to the respective **mOEG$_m$-NH$_2$**. All the synthesized monomers are obtained as white solids after freeze-drying from milli-Q water and fully characterized by means of ^{1}H-NMR, ^{13}C-NMR, and liquid chromatography mass spectrometry (LC–MS) (Figure S1–26).

2.2 | Self-Assembly in Water

The self-assembly behavior of the synthesized molecules is investigated through a combination of spectroscopy, microscopy techniques, and computational molecular modeling. The critical aggregation concentration (CAC) of each monomer in water has been determined through the Nile red assembly assay (Figure 1a) [33]. The Nile red is a fluorescent dye, whose emission undergoes a blue shift upon encapsulation into hydrophobic domains, thus allowing assembly quantification [34]. The CAC of the final molecules is shown to depend both on the HLB and the size of the alkyl-urea spacer, resulting in decreasing CAC values from the more hydrophilic **2-OEG$_m$** to the more hydrophobic **3-OEG$_m$**. Specifically, the CAC of **2-OEG$_3$** is 500 μM, while for **2-OEG$_6$** and **2-OEG$_{12}$** it is 50, and 100 μM, respectively. Remarkably, the higher CAC value of **2-OEG$_3$** might be attributed to its lower HLB value limiting its water solubility, which eventually results in precipitation and uneven distribution of the fluorescent dye within the assemblies in solution. Conversely, **3-OEG$_6$** presents the lowest CAC of 5.0 μM, while the increased hydrophilicity of **3-OEG$_{12}$** results in a CAC of 25 μM. Notably, the CAC values for **1-OEG$_m$** were not determined (N. D.) owing to the lack of hydrophobic domains able to encapsulate the Nile red dye. These results indicate that the assembly of the synthesized molecules is enhanced by the hydrophobicity of the alkyl spacer at equal OEG chain length.

The UV–Vis spectra of **1-OEG$_m$** and **2-OEG$_m$** (Figure 1b) show absorption maxima at 210 nm, 236 nm and 272 nm, which correspond to the non-dimerizing 6[1*H*] UPy tautomer [30, 35]. In contrast, the UV–Vis spectra of **3-OEG$_6$** and **3-OEG$_{12}$** (Figure 1b), present an increased absorbance at 290 nm, represented by a maximum for **3-OEG$_6$** and by a shoulder for **3-OEG$_{12}$**, suggesting the formation of different supramolecular interactions. Fourier-transform infrared (FT-IR) spectroscopy in D_2O revealed significant differences in the amide I region of each monomer, indicating rearrangement in the hydrogen bonding array for the different classes of molecules (Figure 1c). The peak at 1648 cm^{-1} in **1-OEG$_m$** and **2-OEG$_m$** indicates little dimerization of the UPy

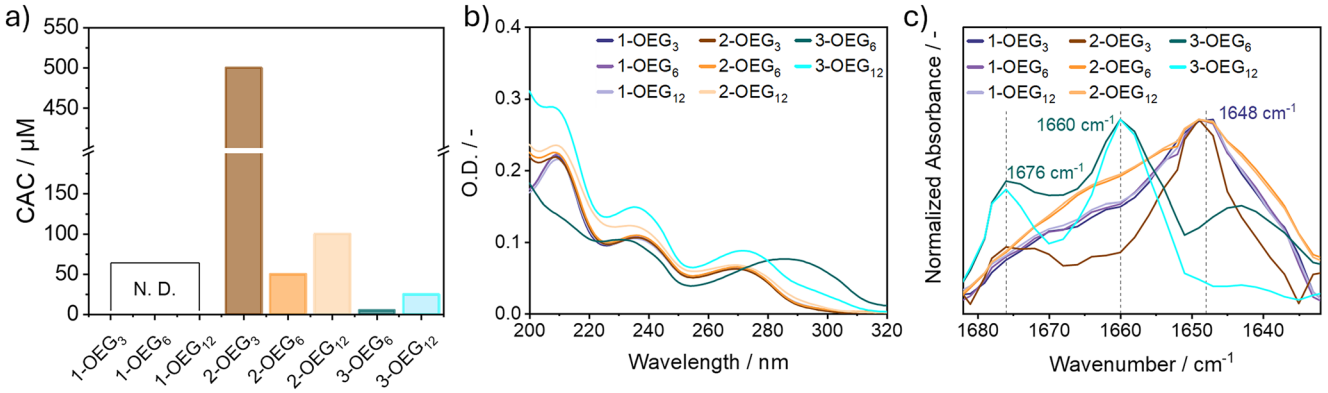

FIGURE 1 | Self-assembly analyses of the assembled monomers in water: (a) Bar chart of the CAC of each monomer derived from the respective Nile red titration curves. (b) UV–Vis spectra of the different monomers ($C = 100\,\mu M$, $T = 20°C$, $l = 1.0\,mm$) and (c) partial FT-IR spectra of the amide I vibration of the assembled UPy monomers in D_2O ($C = 2.5\,mM$, $T = 20°C$, $l = 0.05\,mm$).

core, while the shifted peak at 1660 cm^{-1} in **3-OEG$_m$** represents the hydrogen bonded dimers [30], pointing out an enhanced dimerization for the more hydrophobic class of UPy monomers. Furthermore, the vibration band at 1676 cm^{-1}, observed in the spectra of **3-OEG$_m$** and **2-OEG$_3$**, suggests the formation of additional or competitive intramolecular hydrogen bonding for the monomers featuring lower HLB values.

^{1}H-NMR spectroscopy in D_2O has been employed to determine the visible and mobile fraction of UPy moiety at 500 µM by using a small and constant amount of anhydrous dimethyl sulfoxide (50 µM) as mobile internal standard (Figure S28–35) [36–38]. From the integration of the peak corresponding to the methyl group in position 6 on the UPy ring at 2.02 ppm, the visible fraction of UPy moiety increases with the hydrophilicity of the molecule at room temperature. Indeed, the visible fraction of UPy motif for **1-OEG$_m$** is 72 mol% for **1-OEG$_3$**, 61 mol% for **1-OEG$_6$** and 73 mol%, for **1-OEG$_{12}$**, indicating similar degree of mobility of the UPy core for the three monomers. Conversely, the mobile fraction of UPy moiety for **2-OEG$_m$** is 20 mol% for **2-OEG$_3$**, 36 mol% for **2-OEG$_6$** and 50 mol% for **2-OEG$_{12}$**, while it is 0 mol% for **3-OEG$_6$** and 7.0 mol% for **3-OEG$_{12}$**. These results confirm assembly formation for all the three classes of molecules at 500 µM, however the mobility of the UPy core is strictly affected by the hydrophobicity of the molecule, showing nearly absence of mobility for **3-OEG$_m$** and an increasing mobile fraction from **2-OEG$_m$** to **1-OEG$_m$**. Moreover, a comparison of the chemical shifts of the alkylidene protons on the UPy moiety among the different classes of monomers with identical OEG chain lengths (Figure S28) reveals an upfield shift in the signal as the alkyl spacer length increases. This shift indicates enhanced π–π stacking of the dimers for the more hydrophobic derivatives [25]. Remarkably, no sign of OEG backfolding to the ureido NH of the UPy ring is observed across the various samples, probably due to the hydration of the OEG chains, which hampers the intramolecular hydrogen bonding between those moieties [30].

The morphology of the assemblies formed by each monomer above the CAC has been elucidated by cryogenic transmission electron microscopy (cryo-TEM) (Figure 2), atomic force microscopy (AFM) (Figure S37) and static light scattering (SLS). CryoTEM micrographs of **1-OEG$_m$** (Figure 2a–c) reveals only small, disordered structures which are also observed in the respective AFM height images (Figure S37a–c). Specifically, **1-OEG$_3$** (Figure 2a) and **1-OEG$_6$** (Figure 2b) are visualized as small micelle-like aggregates, while **1-OEG$_{12}$** (Figure 2c) as sheet-like structures. In contrast, the micrographs of the more hydrophobic **2-OEG$_m$** (Figure 2d–f) display significantly different morphologies. For **2-OEG$_3$** (Figure 2d) and **2-OEG$_6$** (Figure 2e), a mixture of small disordered micelles and sheet-like structures is observed, whereas **2-OEG$_{12}$** (Figure 2f) shows small fiber-like structures in addition to micelles. AFM height images (Figure S37d–f) corroborate the cryoTEM micrographs by showing sheet-like structures for **2-OEG$_6$** (Figure S37e) and smaller micelle-like structures for **2-OEG$_{12}$** (Figure S37f). Lastly, the assemblies of **3-OEG$_6$** (Figure 2h) and **3-OEG$_{12}$** (Figure 2i) are predominantly composed of sheet-like structures which appear as a homogeneous coating on the mica substrates (Figure S37h,i).

The scattering plots of the assembled monomers (Figure 2g) exhibit an angular dependence of the Rayleigh ratio (R) across the scattering vector (q) range that differs from the typical patterns observed for fibrillar structures. This confirms the formation of alternative morphologies, such as disk- and sheet-like structures [39]. Notably, the scattering patterns corresponding to **3-OEG$_m$** show the highest R values, followed by **2-OEG$_m$** and **1-OEG$_m$**, while keeping similar slope across the samples. These findings suggest that the nanostructures formed by each monomer present similar anisotropy, but the corresponding size or quantity decreases by increasing the length of the OEG chain and shortening the alkyl spacer length [40].

2.3 | Thermal Stability of the Assemblies in Aqueous Solution

The thermal stability of the assemblies formed by each monomer in solution has been investigated through variable temperature UV–Vis (VT-UV) and ^{1}H-NMR (VT-NMR) spectroscopy (Figure 3) at 100 µM in water and 500 µM in D_2O, respectively.

The UV–Vis spectra of **1-OEG$_m$** (Figure 3a–c) and **2-OEG$_m$** (Figure 3d–f) at room temperature display the same absorption maxima at 210, 236, and 272 nm. On the other hand, the absorption spectrum of **3-OEG$_6$** (Figure 3g) at room temperature shows

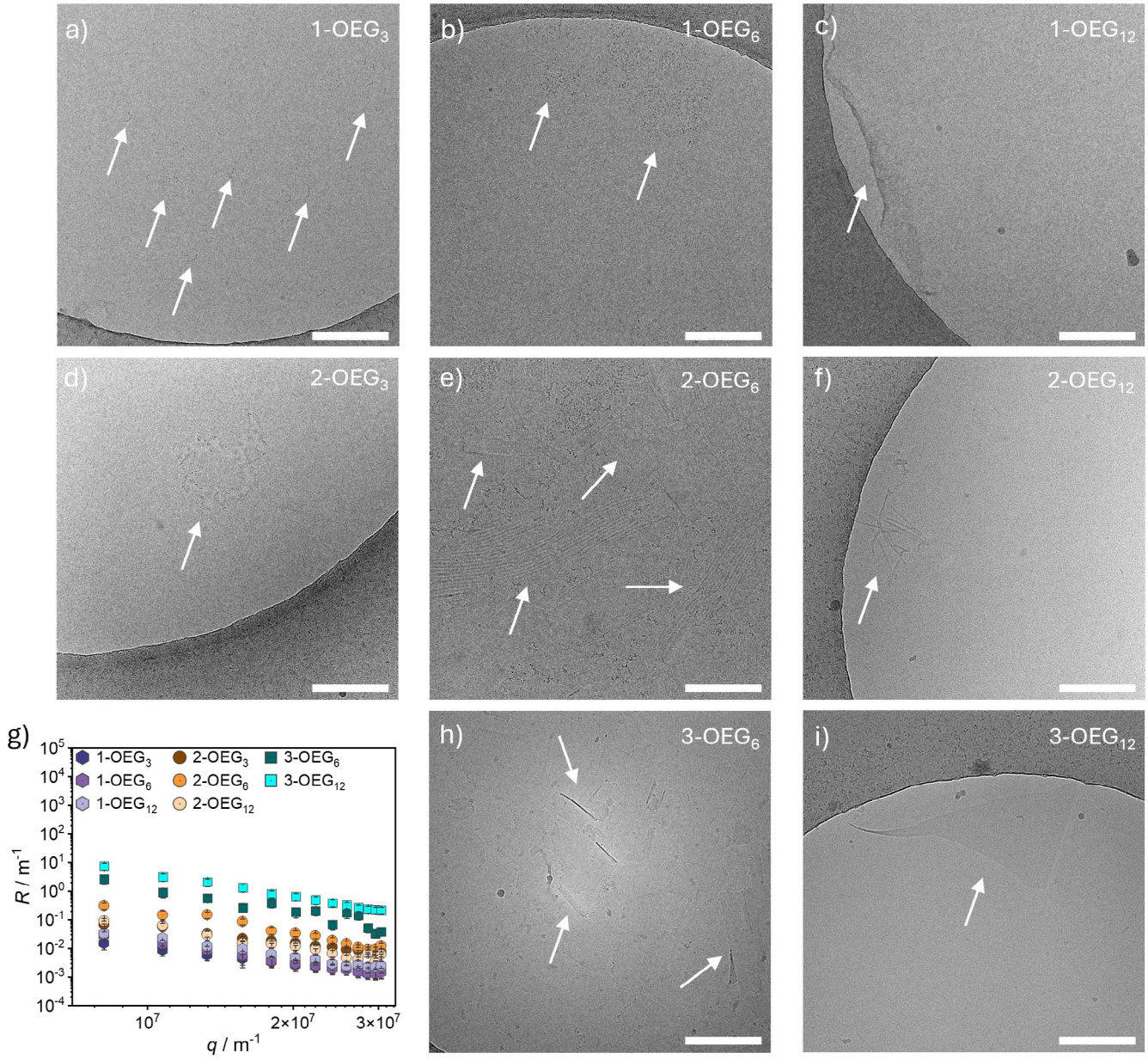

FIGURE 2 | Representative cryoTEM micrographs of (a–c) **1-OEG$_m$**, (d–f) **2-OEG$_m$** and (h–i) **3-OEG$_m$** ($C = 500\,\mu M$). All the micrographs were acquired at a nominal magnification of 56 kx. Scale bars = 200 nm. (g) SLS patterns of the assembled monomers in water ($C = 500\,\mu M$).

absorption maxima at 234 and 290 nm, while the absorption maxima in the spectrum of **3-OEG$_{12}$** (Figure 3h) lay at 208, 236, and 273 nm with a shoulder at 290 nm. By heating the samples from 10°C to 80°C, a small increase in the absorption intensity at 210, 225, and 290 nm along with a small decrease in absorption at 237 nm is observed for **1-OEG$_m$** and **2-OEG$_m$**, suggesting the formation of aggregates through non-covalent interactions, in line with the previous results (*vide supra*). In contrast, the absorption spectra of **3-OEG$_6$** and **3-OEG$_{12}$** present three isosbestic points at 223, 238, and 269 nm for the former and at 224, 248, and 264 nm for the latter over the explored temperature range. The absorption maximum at 290 nm in the spectra of **3-OEG$_6$** shifts to 272 nm at higher temperatures, similar to the blue shift from 274 to 272 nm observed in the absorption spectra of **3-OEG$_{12}$**. In addition, a decrease in the intensity of the shoulder at 290 nm in the absorption spectra of the latter occurs upon heating. The aforementioned hypsochromic shifts suggest the transition from *J*-aggregates to the monomeric state for both the **3-OEG$_m$** at high temperatures [41, 42]. The formation of *J*-aggregates for **3-OEG$_6$** and **3-OEG$_{12}$** is further confirmed by the respective cryoTEM images (*vide supra*), where characteristic sheet-like structures are observed in both cases [41, 42]. Moreover, the cooling curves of the same samples suggest a cooperative mechanism of assembly [43] and the difference in the number of ethylene units results in an elongation temperature of 48°C for **3-OEG$_6$** and 25°C for **3-OEG$_{12}$** respectively, highlighting the importance of the hydrophilic-hydrophobic balance in stabilizing the supramolecular assemblies in water. Conversely, no significant differences are found in the absorbance at 290 nm for **1-OEG$_m$** and **2-OEG$_m$** (Figure S38) over the investigated temperature range, indicating stability of the 6[1*H*] tautomer in solution.

Next, VT-NMR experiments (Figure 3j) have been carried out to confront the thermal stability of the assemblies formed

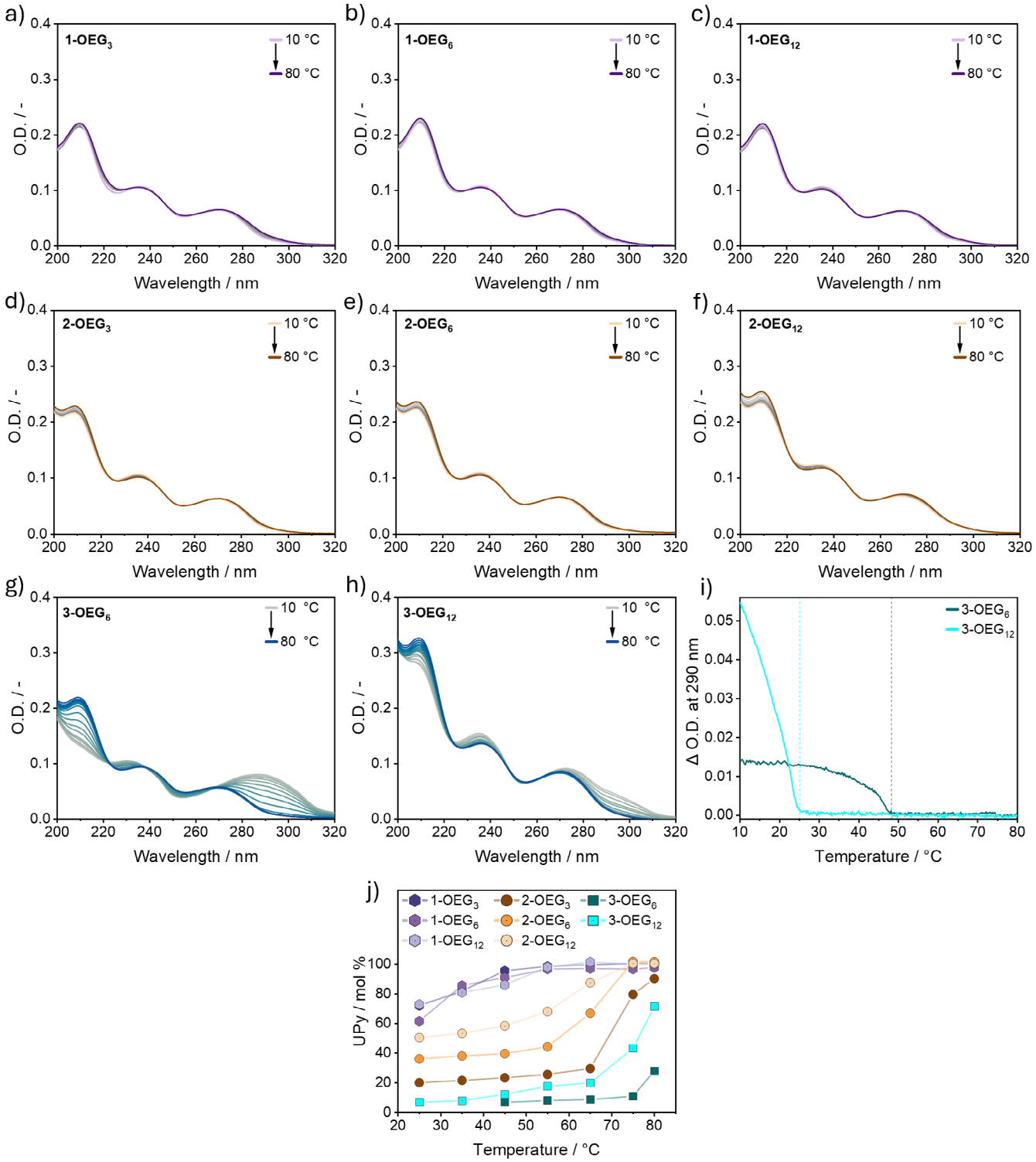

FIGURE 3 | (a–h) Variable temperature UV–Vis spectra of the assembled monomers ($C = 100\,\mu M$, $1\,°C\,min^{-1}$, $l = 1\,mm$) and (i) cooling curves of **3-OEG$_m$** ($0.2\,°C\,min^{-1}$, $l = 1\,mm$). (j) NMR quantification of the fraction of visible UPy in the liquid-like phase for the synthesized molecules ($C = 500\,\mu M$ in D_2O) at different temperatures (25°C–80°C) with anhydrous dimethyl sulfoxide as an internal standard ($C = 50\,\mu M$ in D_2O).

by each monomer at higher concentration (500 μM). The kinetic curves of each monomer indicate a negative correlation between the fraction of visible UPy moiety (mol%) and the hydrophobicity of the molecule across the investigated temperature range. For **1-OEG$_m$**, 100 mol% of visible UPy moiety is achieved above 55°C, while a higher temperature of 75°C is needed to yield 100 mol% of UPy moiety in the liquid-like phase for the more hydrophobic **2-OEG$_6$** and **2-OEG$_{12}$**. Moreover, for **2-OEG$_3$** only 90 mol% of visible UPy is achieved at 80°C, indicating higher stability of the assemblies formed by the more hydrophobic **2-OEG$_3$**. Conversely, for **3-OEG$_6$** and **3-OEG$_{12}$** only 28 and 71 mol% of visible UPy moiety is observed at 80°C, confirming the importance of the hydrophobicity of the monomer in stabilizing the assemblies.

2.4 | Molecular Dynamics Simulations

Molecular dynamics (MD) simulations have been conducted to gain a clearer picture on the factors governing the self-assembly of the different synthesized UPy monomers. Self-assembly MD simulations of 42 randomly dispersed monomers in water have been performed on **1-OEG$_6$** and **3-OEG$_6$**, separately, over a timescale of 1 μs (Figure 4a,b), providing quantitative details on the molecular interactions driving the aggregation of the two monomers featuring extreme opposite HLB values. The difference between the two systems has been quantified by computing the aggregation propensity (AP) parameter [44–46], which evaluates the reduction in solvent accessible surface area (SASA) of the UPy monomers resulting from the self-assembly. In particular, the AP value measures the ratio between the total SASA of N monodispersed monomers ($SASA_{mon}$) and the total SASA of the progressive aggregation state $\left(\sum SASA_{ags}(t)\right)$ along the MD simulation according to the following equation

$$AP(t) = \frac{N_{mon} \times SASA_{mon}}{\sum_{Na} SASA_a(t)} \quad (1)$$

Indeed, upon self-assembly of the monomers, their contact area with the solvent decreases, resulting in an increase in the AP values (Figure 4c).

Consistent with the experimental results, the time evolution of the AP unveils a faster and more pronounced aggregation tendency for **3-OEG$_6$** than for **1-OEG$_6$**. Moreover, as the aggregation of both systems proceeds, the potential energy contributions (Coulomb and Van der Waals), associated to monomer-monomer interactions, lower the energy of the systems due to the attractive interactions between the monomers. By breaking down the energetic contributions of each monomer fragment (UPy core, C_{12} spacer, urea and OEG_6), it is evident that the C_{12} spacer and the urea unit add an additional contribution to the aggregation process of **3-OEG$_6$** (Figure 4d), while the contributions of the UPy core and the OEG_6 chain to the self-assembly of both **1-OEG$_6$** (Figure 4e) and **3-OEG$_6$** (Figure 4d) remain consistent. This explains the higher AP of **3-OEG$_6$** over **1-OEG$_6$**.

A more detailed analysis on the role of the lateral urea in **3-OEG$_6$** (Figure S39) reveals that the interaction energy between the urea and the UPy core, as well as between the urea and the C_{12} spacer fragments, enhances the AP. However, this interaction simultaneously competes with the core–core interactions, ultimately disrupting the 1D-stacking of the UPy cores. These results qualitatively confirm the multidirectional growth of the UPy-based assemblies seen from the self-assembly analyses reported above and support the evidence of *J*-type aggregates formation for the more hydrophobic **3-OEG$_m$**.

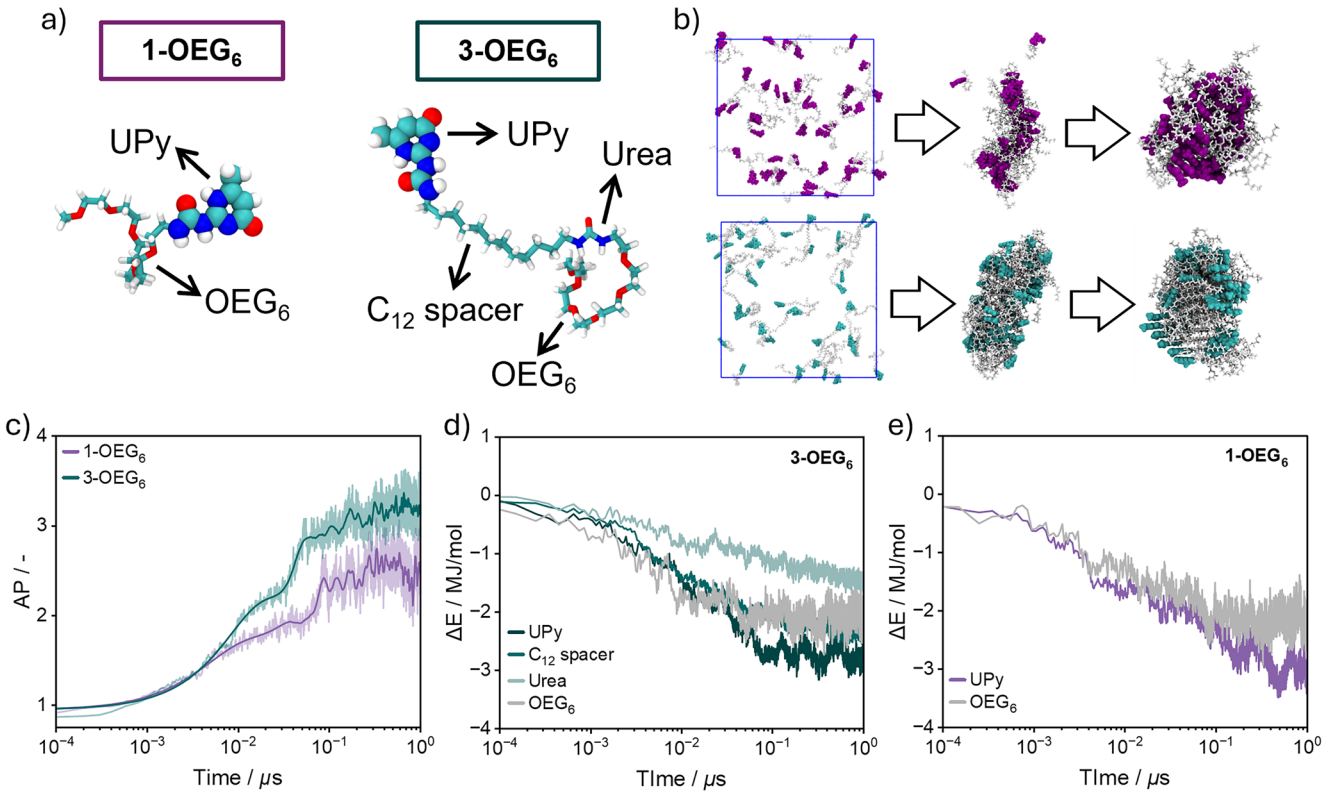

FIGURE 4 | (a) All-atom (AA) models of **1-OEG$_6$** (left) and **3-OEG$_6$** (right) monomers. Atom color code: Oxygen, nitrogen, hydrogen, and carbon atoms are colored in red, blue, white and cyan, respectively. (b) MD screenshots along the 1 μs trajectories, showing the self-assembly of 42 **1-OEG$_6$** (top) and **3-OEG$_6$** (down) monomers. Water molecules are not shown for clarity. (c) Aggregation Propensity (AP) of 42 **1-OEG$_6$** and **3-OEG$_6$** monomers during 1 μs of MD self-assembly simulations. (d, e) Evolution of potential energy terms associated to the interaction between the (d) **3-OEG$_6$** and (e) **1-OEG$_6$** monomer fragments along 1 μs of AA-MD self-assembly simulations. The value ΔE is the energy difference at time t, referred to the initial configuration, when the monomers are well-dispersed in water. Coulomb and Van der Waals interactions are included in the energy calculations.

3 | Conclusion

This study offers a systematic investigation into the self-assembly of eight water-compatible UPy-based supramolecular monomers featuring various HLB values. The results demonstrate that the self-assembly behavior of each monomer and the morphology of the resulting assemblies in water are governed by the monomer design. Notably, while all synthesized monomers undergo self-assembly, the introduction of an alkyl-urea spacer between the UPy core and the OEG chain significantly enhances the self-assembly at equal OEG length, leading to the formation of more rigid supramolecular structures. Interestingly, MD simulations not only confirmed that self-assembly is primarily driven by the combination of UPy dimerization and hydrophobic interactions, but also highlights how the lateral urea competes with the UPy dimerization, thereby destabilizing the 1D elongation of the assemblies and eliciting the formation of *J*-type aggregates featuring a sheet-like morphology. This work enriches the knowledge about the supramolecular polymerization of UPy molecules in water, providing with opportunities towards the development of novel supramolecular biomaterials with tunable properties.

Acknowledgments

The authors acknowledge Dr. Giulia Lavarda and Prof. Bert Meijer for the fruitful discussions. This research was financially supported by the Ministry of Education, Culture and Science (Gravity Program 024.005.020), a NWO VICI grant from the Netherlands Organization for Scientific Research (NWO, VI.C.222.088), and the European Union's Horizon research and innovation program under grant agreement 101079482 ("SUPRALIFE").

Data Availability Statement

The data that support the findings of this study are available on request from the corresponding author upon reasonable request. All data and materials related to the simulation MD trajectories and the analysis conducted herein are available at: https://doi.org/10.5281/zenodo.17582412.

References

1. L. Rijns, M. B. Baker, and P. Y. W. Dankers, "Using Chemistry to Recreate the Complexity of the Extracellular Matrix: Guidelines for Supramolecular Hydrogel–Cell Interactions," *Journal of the American Chemical Society* 146 (2024): 17539–17558.

2. C. M. A. Leenders, M. B. Baker, I. A. B. Pijpers, et al., "Supramolecular Polymerisation in Water; Elucidating the Role of Hydrophobic and Hydrogen-Bond Interactions," *Soft Matter* 12 (2016): 2887–2893.

3. L. Rijns, J. W. Peeters, S. I. S. Hendrikse, et al., "Importance of Molecular and Bulk Dynamics in Supramolecular Hydrogels in Dictating Cellular Spreading," *Chemistry of Materials* 35 (2023): 8203–8217.

4. S. C. Yuan, Z. Álvarez, S. R. Lee, et al., "Supramolecular Motion Enables Chondrogenic Bioactivity of a Cyclic Peptide Mimetic of Transforming Growth Factor-β1," *Journal of the American Chemical Society* 146 (2024): 21555–21567.

5. R. Z. Pavlović, S. A. Egner, L. C. Palmer, and S. I. J. Stupp, "Supramolecular Polymers: Dynamic Assemblies of "Dancing" Monomers," *Polymer Science* 61 (2023): 870–880.

6. Z. Álvarez, A. N. Kolberg-Edelbrock, I. R. Sasselli, et al., "Bioactive Scaffolds With Enhanced Supramolecular Motion Promote Recovery From Spinal Cord Injury," *Science* 374 (2021): 848–856.

7. J. Shi, X. Du, D. Yuan, R. Haburcak, N. Zhou, and B. Xu, "Supramolecular Detoxification of Neurotoxic Nanofibrils of Small Molecules via Morphological Switch," *Bioconjugate Chemistry* 26 (2015): 1879–1883.

8. Y. Feng, R. Mu, Z. Wang, et al., "A Toll-Like Receptor Agonist Mimicking Microbial Signal to Generate Tumor-Suppressive Macrophages," *Nature Communications* 10 (2019): 2272.

9. H. Cui, T. Muraoka, A. G. Cheetham, and S. I. Stupp, "Self-Assembly of Giant Peptide Nanobelts," *Nano Letters* 9 (2009): 945–951.

10. M. P. Hendricks, K. Sato, L. C. Palmer, and S. I. Stupp, "Supramolecular Assembly of Peptide Amphiphiles," *Accounts of Chemical Research* 50 (2017): 2440–2448.

11. E. T. Pashuck and S. I. Stupp, "Direct Observation of Morphological Tranformation From Twisted Ribbons Into Helical Ribbons," *Journal of the American Chemical Society* 132 (2010): 8819–8821.

12. F. Tantakitti, J. Boekhoven, X. Wang, et al., "Energy Landscapes and Functions of Supramolecular Systems," *Journal of Nature Materials* 15 (2016): 469–476.

13. E. T. Pashuck, H. Cui, and S. I. Stupp, "Tuning Supramolecular Rigidity of Peptide Fibers Through Molecular Structure," *Journal of the American Chemical Society* 132 (2010): 6041–6046.

14. S. E. Paramonov, H.-W. Jun, and J. D. Hartgerink, "Self-Assembly of Peptide–Amphiphile Nanofibers: The Roles of Hydrogen Bonding and Amphiphilic Packing," *Journal of the American Chemical Society* 128 (2006): 7291–7298.

15. J. Liu, M. J. G. Schotman, M. M. R. M. Hendrix, et al., "Effects of Structural Variation on the Self-Assembly of Bis-Urea Based Bolaamphiphiles," *Journal of Polymer Science* 59 (2021): 1162–1170.

16. M. M. J. Smulders, A. P. H. J. Schenning, and E. W. Meijer, "Insight Into the Mechanisms of Cooperative Self-Assembly: The "Sergeants-and-Soldiers" Principle of Chiral and Achiral C3-Symmetrical Discotic Triamides," *Journal of the American Chemical Society* 130 (2008): 606–611.

17. S. Cantekin, T. F. A. de Greef, and A. R. A. Palmans, "Benzene-1,3,5-Tricarboxamide: A Versatile Ordering Moiety for Supramolecular Chemistry," *Chemical Society Reviews* 41 (2012): 6125–6137.

18. S. I. S. Hendrikse, L. Su, T. P. Hogervorst, et al., "Elucidating the Ordering in Self-Assembled Glycocalyx Mimicking Supramolecular Copolymers in Water," *Journal of the American Chemical Society* 141 (2019): 13877–13886.

19. M. J. G. Schotman, M. M. C. Peters, G. C. Krijger, et al., "In Vivo Retention Quantification of Supramolecular Hydrogels Engineered for Cardiac Delivery," *Advanced Healthcare Materials* 10 (2021): 2001987.

20. M. M. C. Bastings, S. Koudstaal, R. E. Kieltyka, et al., "A Fast pH-Switchable and Self-Healing Supramolecular Hydrogel Carrier for Guided, Local Catheter Injection in the Infarcted Myocardium," *Advanced Healthcare Materials* 3 (2014): 70–78.

21. M. Putti, T. Mes, J. Huang, A. W. Bosman, and P. Y. W. Dankers, "Multi-Component Supramolecular Fibers With Elastomeric Properties and Controlled Drug Release," *Biomaterials Science* 8 (2020): 163–173.

22. V. Bonito, S. E. Koch, M. M. Krebber, et al., "Distinct Effects of Heparin and Interleukin-4 Functionalization on Macrophage Polarization and In Situ Arterial Tissue Regeneration Using Resorbable Supramolecular Vascular Grafts in Rats," *Advanced Healthcare Materials* 10 (2021): 2101103.

23. J. F. van Sprang, J. G. M. Aarts, M. G. T. A. Rutten, et al., "Co-Assembled Supramolecular Hydrogelators Enhance Glomerulogenesis in Kidney Organoids Through Cell-Adhesive Motifs," *Advanced Functional Materials* 34 (2024): 2404786.

24. S. H. M. Söntjens, R. P. Sijbesma, M. H. P. van Genderen, and E. W. Meijer, "Stability and Lifetime of Quadruply Hydrogen Bonded

2-Ureido-4[1H]-Pyrimidinone Dimers," *Journal of the American Chemical Society* 122 (2000): 7487–7493.

25. M. M. L. Nieuwenhuizen, T. F. A. De Greef, R. L. J. Van Der Bruggen, et al., "Self-assembly of ureido-pyrimidinone dimers into one-dimensional stacks by lateral hydrogen bonding," *Chemistry - A European Journal* 16 (2010): 1601–1612.

26. R. E. Kieltyka, A. C. H. Pape, L. Albertazzi, et al., "Mesoscale Modulation of Supramolecular Ureidopyrimidinone-Based Poly(Ethylene Glycol) Transient Networks in Water," *Journal of the American Chemical Society* 135 (2013): 11159–11164.

27. S. I. S. Hendrikse, S. P. W. Wijnands, R. P. M. Lafleur, et al., "Controlling and Tuning the Dynamic Nature of Supramolecular Polymers in Aqueous Solutions," *Chemical Communications* 53 (2017): 2279–2282.

28. R. Bellan, M. G. T. A. Rutten, X. Lou, et al., "Tuning the Supramolecular Polymerization and Cell Response of Ureidopyrimidinone Monomers by Pushing the Hydrophobic Threshold," *American Chemical Society* 147, no. 25 (2025): 21478–21491.

29. T. F. A. de Greef, M. M. L. Nieuwenhuizen, P. J. M. Stals, et al., "The Influence of Ethylene Glycol Chains on the Thermodynamics of Hydrogen-Bonded Supramolecular Assemblies in Apolar Solvents," *Chemical Communications* 36 (2008): 4306.

30. T. F. A. de Greef, M. M. L. Nieuwenhuizen, R. P. Sijbesma, and E. W. Meijer, "Competitive Intramolecular Hydrogen Bonding in Oligo(Ethylene Oxide) Substituted Quadruple Hydrogen Bonded Systems," *Journal of Organic Chemistry* 75 (2010): 598–610.

31. W. C. Griffin, "Calculation of HLB Values of Non-ionic Surfactants," *Journal of the Society of Cosmetic Chemists* 5 (1954): 249–256.

32. P. Y. W. Dankers, P. J. H. M. Adams, D. W. P. M. Löwik, J. C. M. van Hest, and E. W. Meijer, "Convenient Solid-Phase Synthesis of Ureido-Pyrimidinone Modified Peptides," *European Journal of Organic Chemistry* 2007 (2007): 3622–3632.

33. D. L. Sackett and J. Wolff, "Nile Red as a Polarity-Sensitive Fluorescent Probe of Hydrophobic Protein Surfaces," *Analytical Biochemistry* 167 (1987): 228–234.

34. F. Tantakitti, J. Boekhoven, X. Wang, et al., "Energy Landscapes and Functions of Supramolecular Systems," *Nature Materials* 15 (2016): 469–476.

35. M. Ramaekers, I. de Feijter, P. H. H. Bomans, N. A. J. M. Sommerdijk, P. Y. W. Dankers, and E. W. Meijer, "Self-Assembly of Chiral Supramolecular Ureido-Pyrimidinone-Based Poly(Ethylene Glycol) Polymers via Multiple Pathways," *Macromolecules* 47 (2014): 3823–3828.

36. B. Escuder, M. LLusar, and J. F. Miravet, "Insight on the NMR Study of Supramolecular Gels and Its Application to Monitor Molecular Recognition on Self-Assembled Fibers," *Journal of Organic Chemistry* 71 (2006): 7747–7752.

37. A. R. Hirst, I. A. Coates, T. R. Boucheteau, et al., "Low-Molecular-Weight Gelators: Elucidating the Principles of Gelation Based on Gelator Solubility and a Cooperative Self-Assembly Model," *Journal of the American Chemical Society* 130 (2008): 9113–9121.

38. W. Edwards and D. K. Smith, "Dynamic Evolving Two-Component Supramolecular Gels—Hierarchical Control Over Component Selection in Complex Mixtures," *Journal of the American Chemical Society* 135 (2013): 5911–5920.

39. S. M. C. Schoenmakers, B. W. L. van den Bersselaar, S. Dhiman, L. Su, and A. R. A. Palmans, "Facilitating Functionalization of Benzene-1,3,5-Tricarboxamides by Switching Amide Connectivity," *Organic & Biomolecular Chemistry* 19 (2021): 8281–8294.

40. M. E. J. Vleugels, S. Varela-Aramburu, B. F. M. de Waal, et al., "Choline-Functionalized Supramolecular Copolymers: Toward Antimicrobial Activity againstStreptococcus Pneumoniae," *Biomacromolecules* 22 (2021): 5363–5373.

41. H. v. Berlepsch and C. J. Böttcher, "Cryo-Transmission Electron Microscopy Reveals Mesoscopic H- and J-Aggregates of Near Infrared Cyanine Dyes," *Journal of Photochemistry and Photobiology, A: Chemistry* 214 (2010): 16–21.

42. R. Philip, A. Penzkofer, W. Bäumler, R. M. Szeimies, and C. Abels, "Absorption and Fluorescence Spectroscopic Investigation of Indocyanine Green," *Journal of Photochemistry and Photobiology A: Chemistry* 96 (1996): 137–148.

43. M. Wehner and F. Würthner, "Supramolecular Polymerization Through Kinetic Pathway Control and Living Chain Growth," *Nature Reviews Chemistry* 4 (2020): 38–53.

44. R. Batra, T. D. Loeffler, H. Chan, et al., "Machine Learning Overcomes Human Bias in the Discovery of Self-Assembling Peptides," *Nature Chemistry* 14 (2022): 1427–1435.

45. J. Min, X. Rong, J. Zhang, R. Su, Y. Wang, and W. Qi, "Computational Design of Peptide Assemblies," *Journal of Chemical Theory and Computation* 20 (2024): 532–550.

46. P. W. J. M. Frederix, G. G. Scott, Y. M. Abul-Haija, et al., "Exploring the Sequence Space for (Tri-)peptide Self-Assembly to Design and Discover New Hydrogels," *Nature Chemistry* 7 (2015): 30–37.

Supporting Information

Additional supporting information can be found online in the Supporting Information section. **Data S1:** Supporting Information.